Cross sections and analyzing powers for quasielastic scattering at 795 and 495 MeV using the $(\vec{p}, n)$ reaction

D.L. Prout,[1,3] C. Zafiratos,[1] T.N. Taddeucci,[2] J. Ullmann,[2] R.C. Byrd,[2] T.A. Carey,[2] P. Lisowski,[2] J.B. McClelland,[2] L.J. Rybarcyk,[2] W. Sailor,[2] W. Amian,[2] M. Braunstein,[1,8] D. Lind,[1] D.J. Mercer,[1] D. Cooper,[3] S. DeLucia,[3] B. Luther,[3] D.G. Marchlenski,[3] E. Sugarbaker,[3] J. Rapaport,[4] B.K. Park,[9] E. Gülmez,[5,7] C.A. Whitten, Jr.,[5] C.D. Goodman,[6] W. Huang,[6] D. Ciskowski,[10] and W.P. Alford[11]

[1] *University of Colorado, Boulder, Colorado 80309*

[2] *Los Alamos National Laboratory, Los Alamos, New Mexico 87545*

[3] *The Ohio State University, Columbus, Ohio 43210*

[4] *Ohio University, Athens, Ohio 45701*

[5] *University of California, Los Angeles, California 90024*

[6] *Indiana University Cyclotron Facility, Bloomington, Indiana 47405*

[7] *Bogazici University, PK 2, Bebek 80815, Istanbul, Turkey*

[8] *Eastern New Mexico State University, Portales, New Mexico 88130*

[9] *New Mexico State University, Las Cruces, New Mexico 88003*

[10] *University of Texas, Austin, Texas 78712*

[11] *University of Western Ontario, London, Ontario, Canada N6A 3K7*

(Received 8 July 1994; revised manuscript received 14 April 1995)

Double differential cross sections and analyzing powers over the quasielastic region have been measured using the $(\vec{p}, n)$ reaction on ^{12}C and ^{nat}Pb. The data were obtained at proton energies of 495 and 795 MeV and cover momentum transfers from 1.0–2.1 fm^{-1} at 495 MeV data and from 0.0–3.5 fm^{-1} at 795 MeV. The cross section data are compared to results from a nonrelativistic reaction model that includes contributions from two-step scattering. The analyzing power measurements are compared to a recent relativistic plane-waves model.

PACS number(s): 25.40.Ep, 24.70.+s, 25.40.Kv

I. INTRODUCTION

A prominent feature of (p, n) spectra at nonzero angles is a broad peak centered near the expected energy loss for free nucleon-nucleon (NN) scattering. This peak has been interpreted as the quasielastic charge exchange of a proton from a bound neutron. Since the spin component of the NN force is an important part of the free interaction between nucleons, this component is expected to play a large role in quasielastic (p, n) scattering, as well. In this paper the spin dependence is discussed in terms of the spin-longitudinal $(\sigma \cdot q)$ and spin-transverse $(\sigma \times q)$ components.

The random phase approximation (RPA) with the $\pi + \rho + g'$ residual interaction has been a successful model of isovector nuclear excitations at low momentum transfers [1]. In 1982 a calculation by Alberico *et al.* [2] using this model showed that at large momentum transfers there are significant differences in the collective response of the spin-longitudinal and spin-transverse isovector channels. They predicted that the spin-longitudinal part of the nuclear response is shifted to lower energy loss and enhanced, while the spin-transverse part is shifted to higher energy loss and quenched. These modifications happen beyond about 1 fm^{-1} in momentum transfer, where quasielastic scattering becomes the dominant mode of excitation of the nucleus.

The energy loss of the quasielastic peak versus momentum transfer is shown in Fig. 1 for different probes. The target nucleus is carbon. The solid line represents the kinematics for free nucleon-nucleon (NN) scattering. The open circles are (e, e') data from O'Connell and Schrøder [3]. The quasielastic peak observed in the (e, e') measurements is located at an energy loss larger by about 10 to 25 MeV than that of free NN kinematics. Quasielastic peak positions observed at 2.0 GeV in the $(^3\mathrm{He}, t)$ measurements of Bergqvist *et al.* [4] are plotted as stars. The $(^3\mathrm{He}, t)$ reaction is an isovector interaction $(\vec{\tau} \cdot \vec{\tau})$ and is driven primarily by ρ and π exchange, which excite the spin-transverse and spin-longitudinal isovector responses, respectively. The (e, e') reaction does not excite the spin-longitudinal nuclear response. The shift of the $(^3\mathrm{He}, t)$ peak to lower energy loss with respect to the (e, e') data and with respect to the free kinematic line at around 2 fm^{-1} was interpreted [4] to be due to the collective effects induced by the attractive π part of the underlying residual reaction predicted by Alberico *et al.* [2]. In Fig. 1 are shown the quasielastic peak positions both for the 795-MeV (p, p') data from Ref. [5] (+) and for the (p, n) data from the present experiment (solid circles).

The ratio of spin-longitudinal and spin-transverse responses has been extracted at one momentum transfer (1.75 fm^{-1}) by measuring spin transfer observables over the quasielastic region using the $(\vec{p}, \vec{p}')$ reaction [6,7]. This response ratio reveals little difference between the

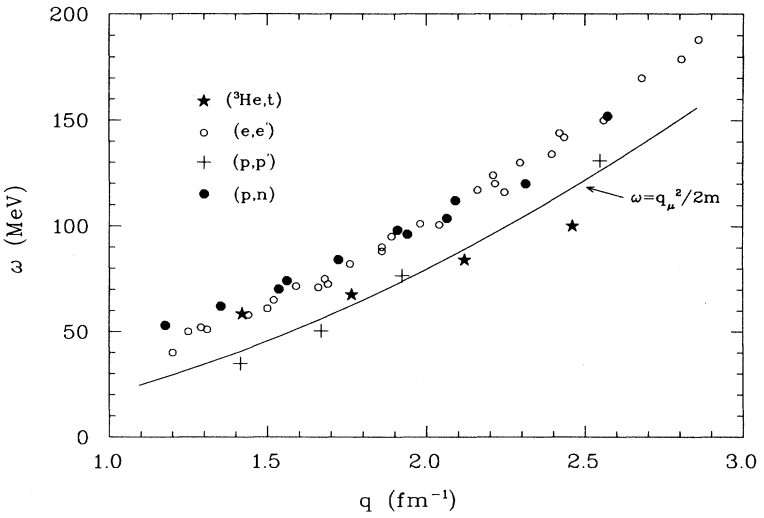

FIG. 1. The quasielastic peak position seen in (e,e') (open circles), (p,p') (+), $(^3\mathrm{He},t)$ (stars), and (p,n) (solid circles) are compared with free NN kinematics (dark solid line). This figure was adapted from Ref. [41].

two responses. This result is at odds with the interpretation of the shift in the $(^3\mathrm{He},t)$ quasielastic peak position. However, the (p,p') reaction is a mixed isovector-isoscalar probe, and the mixture leads to difficulties in the interpretation of the results. On the other hand, ^{3}He itself is a complex probe and it is unclear how this complexity affects the interpretation of the $(^3\mathrm{He},t)$ results at such large momentum transfers.

The (p,n) reaction is ideal for studying the isovector channel, since it suffers from few of the problems of the (p,p') and $(^3\mathrm{He},t)$ reactions. Spin transfer observables for (p,n) reactions have been measured [8], but these measurements are difficult and time consuming and so do not lend themselves to systematic surveys. Alternatively, it is easy to measure the quasielastic cross section, which is still sensitive to collective effects through the position and magnitude of the peak.

In addition to collective effects, quasielastic observables can provide important information concerning the relativistic modification of the NN interaction [9]. This is especially true of the analyzing power, which is also the easiest spin observable to measure.

We report here measurements of cross section and analyzing-power spectra for quasielastic (p,n) reactions at 495 MeV and 795 MeV. The measurements span a broad range of momentum transfer (0.0–3.5 fm^{-1}) where a substantial change in the character of the π residual interaction is expected. Although a variety of target nuclides were studied, we concentrate, in this paper on the ^{12}C and $^{\mathrm{nat}}$Pb data at 795 MeV and the ^{12}C data at 495 MeV.

II. EXPERIMENTAL DETAILS

A. Experiment configurations

The data presented here were obtained in four separate runs at two different experimental areas at the Clinton P. Anderson Meson Physics Facility (LAMPF) in Los Alamos. The 495-MeV data and one 795-MeV data set were obtained with polarized beams available at the Neutron Time of Flight (NTOF) facility. A second 795-MeV data set was obtained at this facility with an unpolarized beam. A third set of 795-MeV data was obtained with an unpolarized beam at the Weapons Neutron Research (WNR) facility.

The 495-MeV data were obtained at the NTOF facility on a flight path of 81 m. Neutron time of flight was measured with respect to a rf signal obtained from the linear accelerator (linac). The effects of energy and time spread in the beam were minimized with a rebunching technique that uses nonaccelerating modules in the linac to produce a time focus at the detector [10]. The resultant overall energy resolution was approximately 2.9 MeV. The natural carbon target used for these measurements had an areal density of 360 mg/cm^2. Carbon spectra were obtained at laboratory scattering angles of 0, 9°, 14°, 16°, 18°, 20°, and 22°. The polarized beam was provided by a Lamb-shift ion source [11] with an average polarization of 77–81 %. The beam polarization was continuously monitored by in-beam polarimeters upstream of the target. The polarization direction was cycled between normal and reverse vertical orientations at approximately two-minute intervals. Beam current was monitored with a secondary emission monitor upstream of the target. Typical beam currents were in the range 3–4 nA, with electronic livetime in the range 86–91 %.

For these initial measurements the NTOF detector system consisted of three liquid scintillator (BC517s) tanks. Each tank had an active volume with dimensions $10 \times 102 \times 107$ cm^3 and was partitioned into ten optically isolated cells viewed on each end by phototubes. An early description of the detector and facility is given in Ref. [12]. A more recent description is contained in Ref. [8]. The detector system was designed as a neutron polarimeter and can be operated in a double scattering detection mode that allows kinematic selection of (n,n) and (n,p) events in the scintillator. When operated in this mode a high degree of background rejection is obtained. Background comes primarily from three sources: γ rays

(from π^0 production), cosmic rays, and frame-overlap neutrons (slow neutrons from preceding beam bursts). In the spectra presented here, background counts are essentially negligible.

The first measurements at 795 MeV were made with unpolarized beam at the WNR facility. Scattering angles up to 7.5° were selected by moving the target along a curved track inside a bending magnet with a horizontal field. For these measurements the spacing of beam micropulses was 5.4 μs, with beam currents ranging from 80 to 120 nA. The flight path at this facility is fixed at 240 m. The neutron detector consisted of a plastic (NE102) scintillation counter with dimensions of $25.4 \times 50.8 \times 4.45$ cm^3. Neutron time of flight was measured with respect to a time signal generated by a nonintercepting beam pickoff installed upstream of the target chamber. The energy resolution for this experiment was about 3 MeV and livetimes ranged from 85% to 95%. The targets were natural carbon (44 mg/cm^2) and natural lead (60 mg/cm^2). Details concerning the WNR setup are given in Ref. [13].

A 618 m flight path was used for the first set of 795-MeV data obtained with the NTOF facility. This long flight path was dictated by the resolution requirements of a different set of measurements. The micropulse spacing of the unpolarized proton beam was 5.0 μs and the beam current ranged from 15 to 40 nA. Time of flight was measured with respect to a time signal generated by a beam pickoff similar to the one used at the WNR facility. The detector configuration was essentially identical to that used for the 495-MeV measurements.

The second set of 795-MeV measurements at the NTOF facility was performed on a flight path of 170 m and utilized an additional plane of plastic scintillators. This fourth plane consisted of six solid plastic scintillator (BC408) bars with dimensions of $10 \times 15 \times 102$ cm^3. These measurements also represent the first production use of polarized beam from the new Optically Pumped Polarized Ion Source (OPPIS) [14]. The beam quality for these measurements was rather poor, with an average polarization of about 45%. The polarization state was cycled between plus and minus vertical orientations at 2 min intervals. The spacing between beam micropulses was 198.8 ns with an average current that ranged from 2 to 20 nA. Neutron time of flight was measured with respect to a rf signal derived from the linac. The energy resolution for this set of data was about 4.5 MeV. Data were obtained at scattering angles of 0, 9°, 12°, 15°, and 18°. Targets consisted of natural carbon (98.9% ^{12}C) (1770 mg/cm^2), natural lead (1730 mg/cm^2), CD_2 (780 mg/cm^2), ^{7}Li (720 mg/cm^2), ^{90}Zr (25.5 mg/cm^2), ^{27}Al (90 mg/cm^2), and ^{58}Ni (90 mg/cm^2). Only carbon and lead spectra were measured at all angles.

B. Data reduction and cross section normalization

The integrated output from a secondary emission monitor upstream from the target served to normalize NTOF runs to each other. For the WNR facility the output of the beam pickoff device was randomly sampled. The signal from this device was integrated to produce a signal proportional to the number of protons that passed through the pickoff for a given beam pulse. These signals were stored in a multichannel analyzer and read out at the end of each run. This provided the average number of protons per beam pulse, and allowed the total charge to be computed for each run. In addition, the energy spectra were corrected to account for the attenuation of neutrons along the flight path. While the attenuation was as large as 30% for the longest flight path, the energy dependence is very weak for neutrons in the energy range 100–800 MeV so this led to only a small (2%) relative correction.

Absolute normalization of the data was obtained by normalizing 0° neutron yields from the ^{7}Li$(p,n)^7$Be(g.s. + 0.42 MeV) reaction to a standard center-of-mass (c.m.) cross section (27 $\frac{\text{mb}}{\text{sr}}$). The 0° cm cross section for this reaction has been shown to be constant over the energy range from 80 to 795 MeV [15]. Detector efficiencies based upon this normalization procedure are approximately constant over the energy range 318–795 MeV. This result is consistent with an absolute measurement of the detector efficiency using tagged neutrons [16].

We identify two types of systematic uncertainties associated with our measurements: (a) uncertainties affecting the relative normalization of the data such as current integration and target thickness, and (b) uncertainty due to the absolute normalization of our data to the ^{7}Li activation. A 6% uncertainty has been associated with the beam integration. A value of 5% is used for the uncertainty in target thickness. There is a 3% uncertainty in the absolute ^{7}Li activation measurement [15]. Adding these in quadrature, we estimate a systematic uncertainty of about 9%.

An independent check of the normalization and of the uncertainties associated with the current integration and target thickness is provided by comparing our integrated cross sections with the cross section measurements from Refs. [17–20]. The (p,n) measurements from Refs. [17–19] were performed using a proton recoil technique at the LAMPF Nucleon Physics Lab (NPL). This technique is described in Ref. [17]. The (p,n) measurements of Ref. [20] were made using time of flight techniques at WNR.

The data from Ref. [20] were normalized to the 0° Pb spectrum of Ref. [17]. We have connected our cross section data to the data of Ref. [20] and to the data from the NPL facility through this Pb spectrum. Our data were integrated over the ranges specified in Refs. [17–19] (approx. $0 < \omega < 140$ MeV). Our cross section results on ^{12}C, ^{7}Li, and ^{2}H agree with those of Ref. [20] to better than 8% at all angles for which we have overlapping data. Similarly our ^{12}C and ^{27}Al data agree with those of Refs. [17,19] to better than 4%. These comparisons are consistent with our estimate of about 8% uncertainty associated with relative normalization.

When our data are normalized via the ^{7}Li activation, our neutron yields are greater than those of Refs. [17–19] by a factor of about 1.6 on all targets. Although we have tried to understand this large discrepancy, we do not have a simple explanation for it. A more detailed discussion of the alternative normalization procedures for 795-MeV (p,n) data is given in Ref. [21].

The quasielastic cross section for the ^{2}H(p,n) reaction also provides a check of the absolute normalization. Because of the large momentum transfers encountered in this experiment, the three nucleons involved in the ^{2}H(p,n) reaction will have large relative momenta. Pauli blocking and final state interactions which are important at 0° may be ignored at these angles and the differential cross section in this reaction should be approximately equal to the free charge-exchange NN differential cross section. For this comparison we use NN cross sections extracted from the phase-shift solution of Arndt and Roper [23]. The consistent procedure described in Ref. [22] was used to determine the ranges for integrating the ^{2}H data.

Good agreement is obtained between the ^{2}H(p,n) cross section and the free charge-exchange cross section at 495 MeV and 18° [8]. However, at 795 MeV the integrated ^{2}H cross sections at laboratory angles of 9°, 12°, 13.5°, 15°, and 18° are about 20% higher than the NN values. Because the theoretical calculations are based on the phase-shift solutions of Ref. [23], these calculations will appear artificially low (20%) when compared to our data.

We note that a subset of the ^{12}C data has appeared in Ref. [24]. The data shown in that paper used a preliminary normalization and should be multiplied by 1.6 to be consistent with the present results.

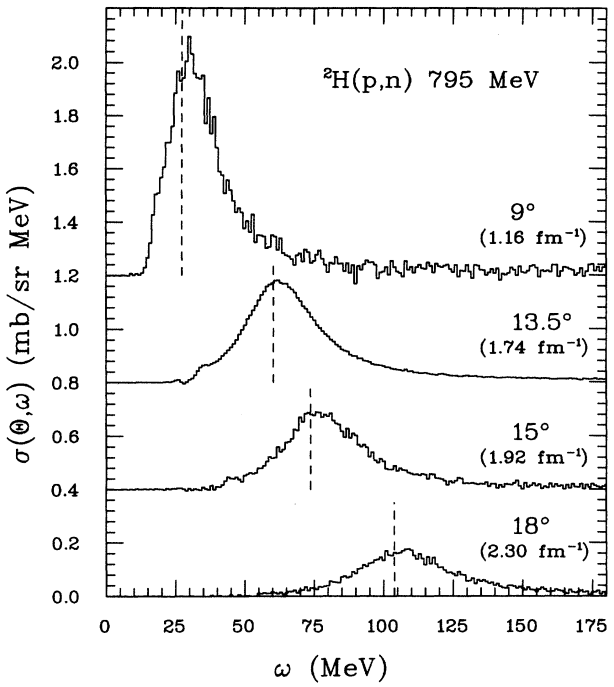

FIG. 2. Energy loss spectra for the ^{2}H(p,n) reaction at 795 MeV are shown at four angles. These angles correspond to momentum transfers from about 1.2 to 2.3 fm^{-1}. The vertical dashed line is the expected energy loss for free NN scattering. Each spectrum is offset vertically from the one below it by 0.40 mb/sr MeV.

III. RESULTS

A. General features

The simplest model of quasielastic scattering is that of a single bound nucleon being knocked out of a nucleus with the remaining nucleons acting as spectators. This leads to the following nonrelativistic kinematic expression for the energy loss of the projectile:

$$\omega = \frac{q^2}{2m} + \frac{\vec{p}_{\text{target}} \cdot \vec{q}}{m} , \tag{3.1}$$

where q is the momentum transfer, ω is the energy loss, and p_{target} is the struck nucleon's internal momentum. The first term describes free NN scattering. The relativistic version of this term is the solid line plotted in Fig. 1. The second term shows that the peak widens with momentum transfer due to the motion of the struck nucleon. Other effects contribute to the energy loss of the projectile, which have been described in various ways by different authors and are discussed below. We use expression (3.1) to establish that we are observing quasielastic scattering and to illustrate the general features of the cross section in this region.

Figure 2 shows ^{2}H(p,n) data at 795 MeV for a range of scattering angles. These spectra were obtained by subtracting the ^{12}C(p,n) contributions from the CD$_2(p,n)$ spectra. The vertical dashed line shows the expected energy loss for free NN scattering at each angle. The ^{2}H(p,n) spectra represent scattering from a very loosely bound neutron. Fermi motion of the struck neutron causes the peak to widen with momentum transfer, as expected from Eq. (3.1). There is a small shift of about 2 MeV. This same shift was observed in previous ^{2}H(p,n) data obtained at 495 MeV and 18° [8].

The ^{12}C(p,n) data are shown in Figs. 3 and 4 for small angles at 795 MeV. Low-excitation discrete states dominate the carbon spectra for angles less than 6°. At 6° a structure appears that follows the kinematics for free scattering but is located at larger energy loss. This broad peak widens as the angle increases, just as with the ^{2}H(p,n) reaction. This kinematic behavior is in contrast to that for discrete states, which move with the kinematics of a nucleon striking a heavy target. This broad structure is therefore identified as quasielastic scattering.

Carbon data at large momentum transfers (up to 3.5 fm^{-1}) are shown in Fig. 5. Because the quasielastic peak spreads with momentum transfer, it becomes more difficult to clearly identify the peak position at these large angles. In addition, it is believed that other processes such as two-step scattering begin to make up a large part of the cross section, which further obscures the quasielastic peak.

Figure 6 shows ^{12}C(p,n) spectra at 495 MeV over a range of momentum transfers that corresponds closely to that of the 795-MeV data in Fig. 4. The 495-MeV and 795-MeV spectra are remarkably similar. This energy independence is expected; the Glauber approximation (discussed below) suggests that the proton probes

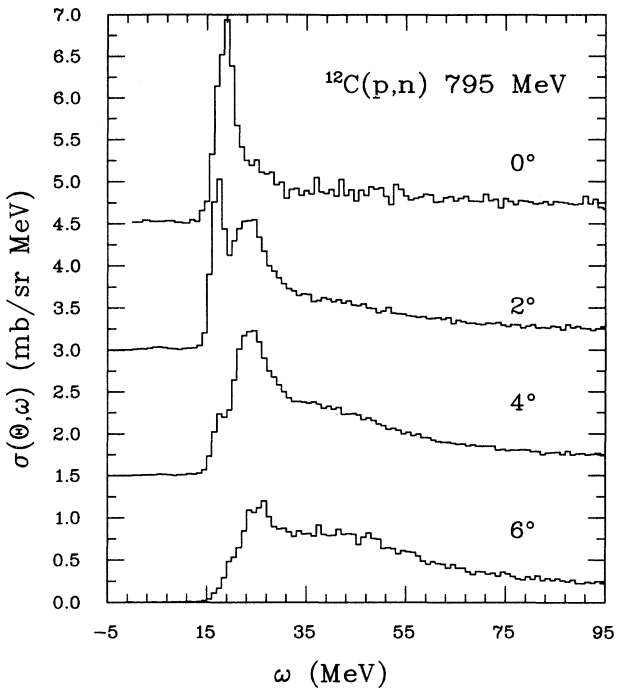

FIG. 3. Energy loss spectra for the $^{12}C(p,n)$ reaction at 795 MeV and at small momentum transfer. The angles correspond to momentum transfers from about 0.0 to 0.77 fm^{-1}. The data show that discrete nuclear states dominate the spectra at these small angles. Each spectrum is offset vertically from the one below it by 1.5 mb/sr MeV.

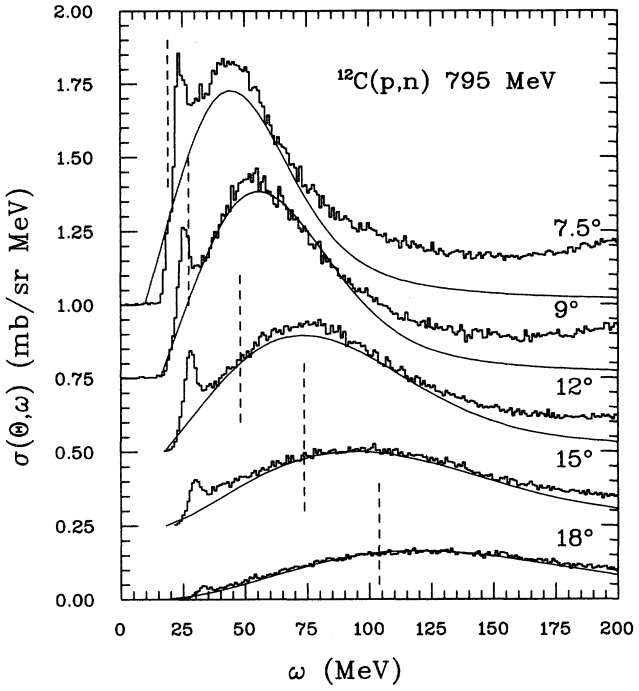

FIG. 4. Energy loss spectra for the $^{12}C(p,n)$ reaction at 795 MeV at moderate momentum transfers. The angles correspond to momentum transfers from about 0.97 to 2.3 fm^{-1}. The vertical dashed line is the expected energy loss for free NN scattering. The quasielastic peak dominates the spectra at these angles. The solid curves are the slab model calculations added to the two-step calculation and multiplied by 1.8. Each spectrum is offset vertically from the one below it by 0.25 mb/sr MeV.

the nucleus at nearly the same nuclear matter density at both energies.

Cross section spectra obtained for the $^{nat}Pb(p,n)$ reaction at 795 MeV are shown in Fig. 7. These data were obtained at the same angles as those of the 795-MeV carbon data in Fig. 4. These data are quite similar to those for ^{12}C, except for the absence of a cutoff in the low-excitation energy region. This cutoff appears in the carbon data because of the large threshold energy (18.1 MeV) required for the $^{12}C(p,n)$ reaction. The threshold energy is only 3.7 MeV for the $^{208}Pb(p,n)$ reaction; nevertheless, the quasielastic peak appears at nearly the same energy loss for the two reactions.

In order to obtain a better estimate of the quasielastic peak position we have fitted the shape of the quasielastic region using two methods. Because the slab model gives a good description of the shape of the peak, we have fitted the quasielastic peak in a small region around the peak. We have also performed a fit to the parametrization of the quasielastic region as given in Ref. [25]. The quasielastic peak shape is characterized as a product of a Lorentzian and an exponential function. Examples of the fits to this parametrization are shown in Fig. 8. In both fits the maximum value of the fit curve was used as the peak position. The uncertainty in the value of the peak position was determined by the difference in the two fitting methods. This difference was typically 2–3 MeV.

In a recent article concerning quasielastic scattering [26] fits have been used to extract the Fermi momentum and peak position of the one-particle–one-hole ($1p$-$1h$) portion of the nuclear response in the quasielastic region. We do not do this here because we believe there may be a large component of the cross section at these energies resulting from multiple scattering or $2p$-$2h$ excitations. Extracting the $1p$-$1h$ portion of the cross section is very dependent on the shape and magnitude of this background. Since our model of this background is only schematic, we cannot reliably determine the $1p$-$1h$ part of the cross section.

A summary of the peak positions obtained for ^{12}C and ^{nat}Pb is shown in Fig. 9. In this figure, the difference between the energy loss at the peak of the quasielastic distribution and the energy loss for free NN scattering at the same angle is plotted versus momentum transfer. A value of zero corresponds to the solid line in Fig. 1. Both the ^{12}C data and the ^{nat}Pb data show essentially the same shift of about 20 MeV with respect to free kinematics. We do not see the dramatic "softening" of the quasielastic peak across the free NN kinematic line that appears in the $(^3He,t)$ data.

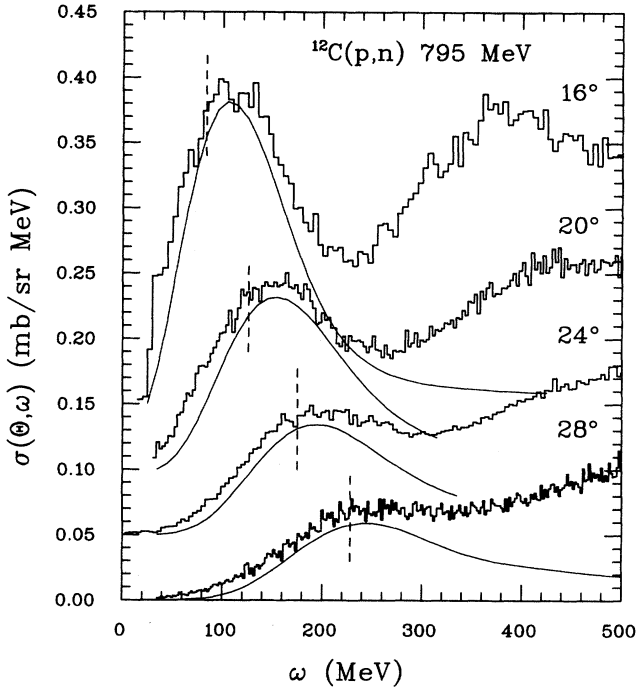

FIG. 5. Energy loss spectra for the $^{12}C(p,n)$ reaction at 795 MeV at large momentum transfers. The angles correspond to momentum transfers from about 2.0 to 3.5 fm^{-1}. The vertical dashed line is the expected energy loss for free NN scattering. The quasifree Δ peak is seen at large energy loss. The solid curves are the slab model calculations added to the two-step calculation multiplied by 1.8. Each spectrum is offset vertically from the one below it by 0.05 mb/sr MeV.

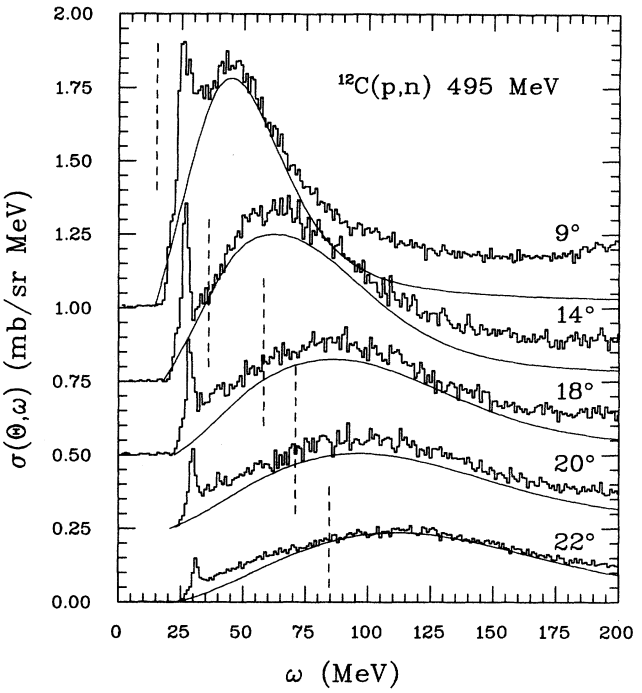

FIG. 6. Energy loss spectra for the $^{12}C(p,n)$ reaction at 495 MeV at momentum transfers close to those of Fig. 4. The angles correspond to momentum transfers from about 0.86 to 2.1 fm^{-1}. The solid curves are the slab model calculations added to the two-step calculation and multiplied by 1.3. Each spectrum is offset vertically from the one below it by 0.25 mb/sr MeV.

In Fig. 10 the target dependence of the quasielastic peak is shown at 15° (1.9 fm^{-1}) for both (p,p') and (p,n) reactions. For the (p,n) reaction, except for ^{2}H and ^{7}Li, the peak position is located at about 20 MeV higher energy loss than free NN scattering at this angle.

B. Comparison of the (p,n) reaction to (p,p')

Comparison of quasielastic scattering in the (p,p') and (p,n) reactions is interesting because the (p,p') quasielastic process is predominantly isoscalar whereas the (p,n) reaction is purely isovector. Figure 11 shows spectra for both reactions at 15° (1.9 fm^{-1}) at 795 MeV. The (p,p') data are from Ref. [5] and have been renormalized as specified in Ref. [28].

Two features of this comparison are apparent. The peak position for (p,p') quasielastic scattering closely matches that for free NN scattering and the magnitude of the (p,p') cross section is much larger than the (p,n) cross section. The large (p,p') cross section reflects the fact that this reaction is dominated by the isoscalar nonspin-flip part of the NN interaction. The cross section for this part of the NN interaction at 795 MeV is

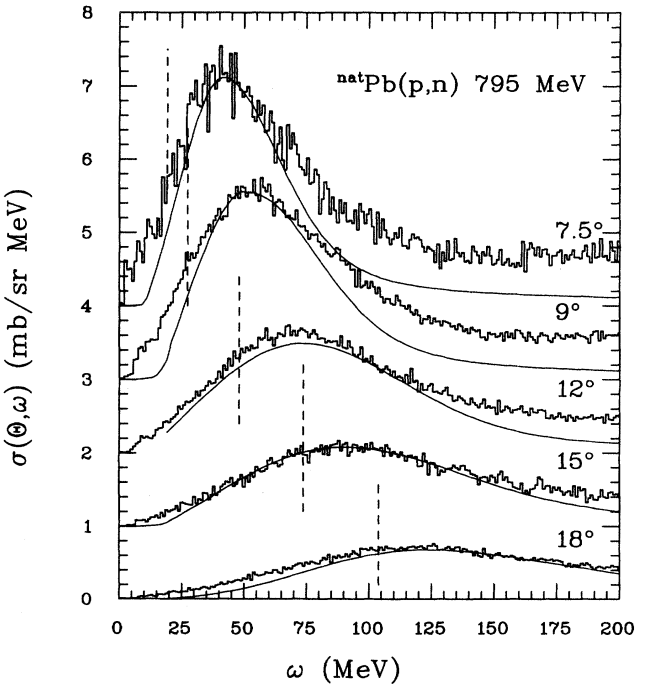

FIG. 7. Energy loss spectra for the $^{nat}Pb(p,n)$ reaction at 795 MeV at the same momentum transfers as those in Fig. 4. The solid curves are the slab model calculations added to the two-step calculation multiplied by 1.8. Each spectrum is offset vertically from the one below it by 1.0 mb/sr MeV.

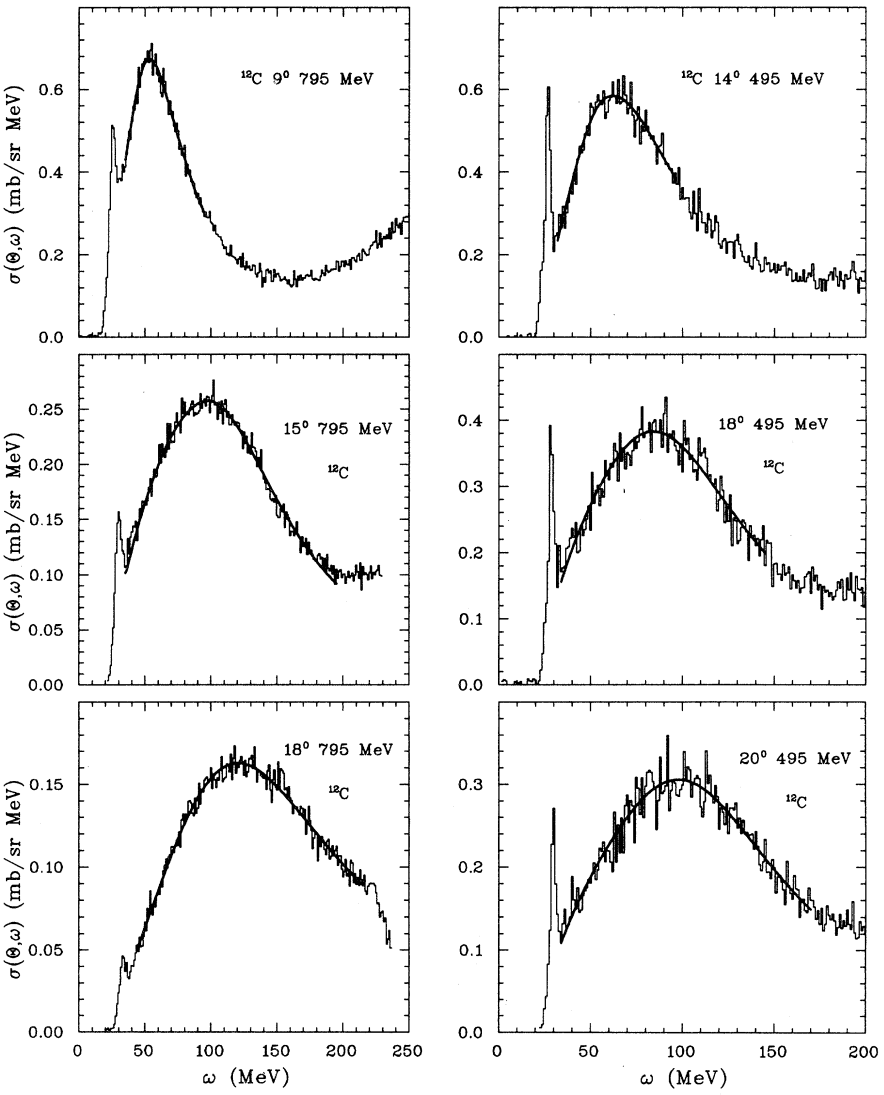

FIG. 8. In this figure is shown a sample of the fits to the parametrization of the quasielastic peak given in Ref. [25]. On the left are 795-MeV carbon data, while on the right are the 495-MeV carbon data. The "peak" position of the quasielastic region used in Figs. 9 and 10 was determined by the position of the maximum value of the fit curves.

nearly a factor of 10 larger than any part of the isovector interaction.

An appealing explanation for the shift of the (p,n) from the free kinematic line is that it represents the average energy needed to knock the struck nucleon from the nucleus. However, this explanation is known to be incorrect; a similar shift due to separation energy should be seen in (p,p') quasielastic scattering and this is not observed. The large shift in the quasielastic peak observed in (e,e') scattering (Fig. 1) was once also attributed to "binding" energy [29,30]. This interpretation was shown to be incorrect by Rosenfelder [31]; in the absence of distortions and correlations the quasielastic peak position should appear on the free kinematic line.

A thorough study of the quasielastic peak position for the (p,p'), (p,n), and (e,e') reactions in relation to standard RPA distorted-wave impulse approximation (DWIA) calculations is given in [24,32]. These authors demonstrate that distortions can cause the peak to shift in (p,n) and (p,p') reactions. However, they obtain a target dependence to the shift in the (p,n) case that is not observed.

A recent alternative explanation for the difference in peak positions between the (p,n) and (p,p') reactions has been given by Pandharipande *et al.* [33] and Wambach [34]. Wambach defines the quasielastic peak as the average energy loss over the quasielastic region. Sum rules, which can be calculated very accurately, may then be used to determine the quasielastic peak position. Both Pandharipande *et al.* [33] and Wambach [34] have been able to describe the difference in the peak positions for the (p,p') and (p,n) reactions in terms of these energy weighted sum rules. Details concerning these explanations may be found in Refs. [33,34]. These calculations show that the difference in peak position is due to differences in collective effects in the isovector (p,n) reaction and the predominantly isoscalar (p,p') reaction. The strong correlations are in the isovector channel pushing

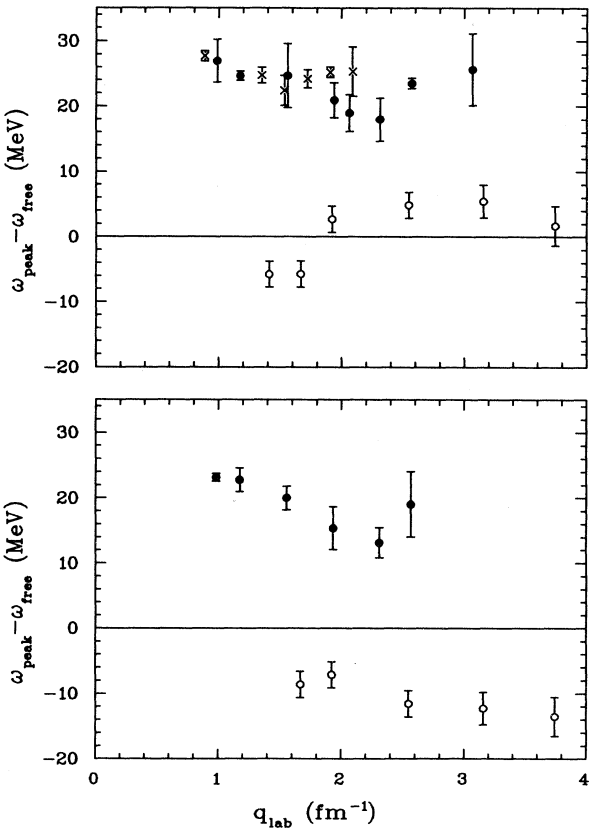

FIG. 9. The difference between the measured quasielastic peak position and the position expected from free NN kinematics is shown for ^{12}C (top panel) as a function of momentum transfer. The solid points are for the (p,n) reaction at 795 MeV and the crosses are for the same reaction at 495 MeV. The open points are the peak positions for the (p,p') reaction on ^{12}C from Ref. [5]. The bottom panel shows the same quantity plotted for ^{nat}Pb using the (p,n) reaction (solid circles) and the (p,p') reaction (open circles). The uncertainty on the (p,p') data represents half the bin width of the data in Ref. [5].

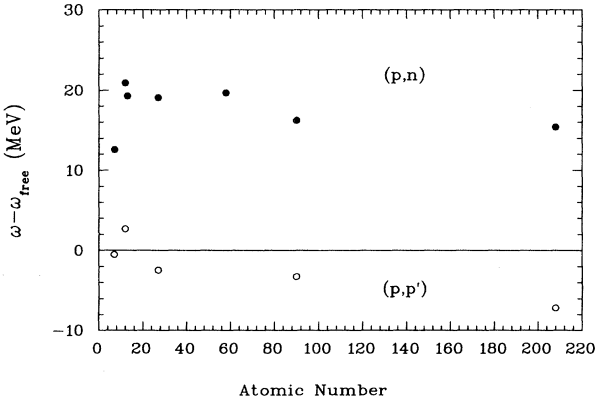

FIG. 10. The difference between the measured quasielastic peak position and the position expected from free NN kinematics is shown as a function of atomic mass for a number of targets at one angle (15°). The solid points are for the (p,n) reaction at 795 MeV and the open points are for the (p,p') reaction from Ref. [5] at 795 MeV.

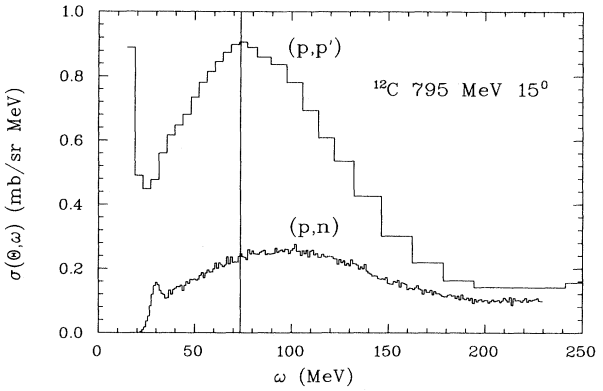

FIG. 11. Energy loss spectra for the (p,p') and (p,n) reactions are compared for ^{12}C at 15° and 795 MeV. The vertical line is the expected energy loss for NN scattering at this angle. The (p,p') data are from Ref. [5] and scaled as specified in [28].

the (p,n) peak to larger energy loss.

The quasielastic peak position for the (p,p') reaction on other targets and at other angles is plotted in Figs. 9 and 10 along with the (p,n) peak positions. All of the (p,p') data are consistent with NN kinematics except for ^{nat}Pb, which appears at even lower energy loss.

IV. SIMPLE MODELS OF QUASIELASTIC SCATTERING

A. Single-step scattering

Because of the high energies involved here, an appropriate basis for modeling the quasielastic process is the eikonal approximation. In this type of model, the double differential cross section may be factored into a distortion term represented as an effective number of nucleons, the differential cross section for free NN scattering, and the nuclear response per nucleon.

The nonrelativistic Fermi-gas model [35], which replaces the nucleus with infinite nuclear matter, has been used to describe roughly the major features of the inclusive quasielastic (e,e') cross section [29]. In the absence of Pauli blocking, this model produces a parabolic shaped energy spectrum, which widens with increasing momentum transfer.

Hadronic probes such as the (p,n) reaction are strongly absorbed and the quasielastic reaction is therefore surface peaked. A better description than the Fermi-gas model for hadronic probes, which takes account of the surface nature of the reaction, is the semi-infinite slab (SIS) model. The slab model incorporates some of the effects of the surface peaking directly into the nuclear responses [36]. This model has three notable features: it redistributes some of the strength of the single-scattering response into a long tail, it smooths the response in the low-excitation Pauli-blocking region, and it includes the effects of the binding energy of the nucleus through a

Woods-Saxon potential.

An alternative one-step model is the relativistic plane-wave impulse approximation (RPWIA). This model employs infinite nuclear matter and accounts for distortions through an overall attenuation factor as with the slab model. This model takes account of the changes in the NN amplitudes due to density dependent changes in the nucleon mass. This has been important for explaining (p,p') elastic scattering data [9]. The inelastic (p,n) analyzing power is sensitive to the form of the pseudoscalar invariant term in the NN amplitude, which is not easily accessible via elastic (p,p') scattering [9]. For the preferred form of the pseudoscalar invariant, the analyzing power for quasielastic (p,n) scattering is predicted to be more positive than the corresponding free NN value. This prediction is tested here with a comparison to a recent calculation of Horowitz and Piekarewicz [37]. In their calculation the in-medium nucleon masses are $m^* = 0.85m$, due to the strong scalar potential that is predicted by relativistic models of the nucleus. With the pseudovector form of the pseudoscalar invariant these smaller masses cause the analyzing power to increase. This calculation is similar to earlier calculations by Horowitz and Murdock [9] except that it contains RPA correlations generated from π and ρ exchange. These correlations cause a slight decrease in the value of the analyzing power compared with the results of Ref. [9].

Full finite-nucleus distorted-waves calculations including correlations in the RPA have recently been reported [41,42]. However, to describe the general features of the data the slab model is adequate. Because of the availability of the RPWIA and slab model codes, we compare our data primarily to these less detailed calculations. In the discussion section, the slab model calculation is compared with the calculation of Ref. [42] at one energy and angle.

B. Two step

It has been suggested that two-step scattering should contribute significantly to (p,n) quasielastic observables [36]. To assess the potential contribution of two-step scattering, we have modeled this process in the eikonal approximation.

The two-step contribution can be computed as an integral over all possible ways of doing two one-step quasielastic excitations, multiplied by a factor which determines the effective number of nucleon pairs in the nucleus. For (p,n) scattering a single charge-exchange scattering is preceded or followed by an elastic scattering. Both possibilities must be included in the calculation.

In the calculations presented here each of the one-step excitations were calculated with a free Fermi-gas response with no correlations. More detailed calculations have been done using the slab model [36,38]. However, these slab model calculations produce distributions similar in shape to those obtained from simpler Fermi-gas response. More details of the two-step calculations are given in Refs. [21,38].

The calculated two-step scattering cross section is a long flat curve as a function of energy loss. The magnitude of this two-step cross section does not change very much over the angular range covered in this paper. However, the single-step cross section decreases rapidly with angle because the driving NN amplitudes decrease. Because of this, two-step scattering processes play a more important role as the scattering angle increases.

C. Distortion

The strong absorption of the incoming proton is incorporated into the models discussed here through multiplicative factors. This is the only distortion effect included in these models. For the slab model and the RPWIA, these factors represent the effective number of nucleons $N_{\rm eff}$ that can participate in the reaction, while for the two-step calculation the distortion factor represents the effective number of nucleon pairs, $N_{\rm double}$. Absorption causes the reaction to be surface peaked and thus the projectile interacts at a relatively low nuclear density.

Distortion factors have been evaluated for each nucleus using the Glauber approximation [36]. In this approximation, the cross section for n scatterings is [38]

$$\sigma^n = \int d^2b \frac{1}{n!}[T(b)_{\rm elastic}]^n e^{-T(b)_{\rm tot}} \tag{4.1}$$

with

$$T(b)_{\rm elastic} = \int_{-\infty}^{\infty} dz \rho(z,b)\sigma_{\rm elastic}$$

and

$$T(b)_{\rm tot} = \int_{-\infty}^{\infty} dz \rho(z,b)\sigma_{\rm tot},$$

where b is the impact parameter, z is the straight path of the projectile, $T(b)$ is the target thickness at impact parameter b, and ρ is the Fermi function with parameters for each nucleus taken from Ref. [39]. The effective number of neutrons is given for single-step scattering by

$$N_{\rm eff} = \frac{N}{A}\frac{\sigma^1}{\sigma_{\rm elastic}}, \tag{4.2}$$

where N is the neutron number, A is the atomic number, and σ^1 refers to expression (4.1) with $n = 1$. The values of $\sigma_{\rm elastic}$ and $\sigma_{\rm tot}$ that we use here are in-medium values which are about 80% of the free values [36,40]. At 495 MeV, $\sigma_{\rm tot}$ is about 26 mb, while $\sigma_{\rm elastic}$ is 22 mb. The resulting value of $N_{\rm eff}$ for ^{12}C at 495 MeV is 2.2 and for $^{\rm nat}$Pb it is 9.7. At 795 MeV the effective number of neutrons is 1.85 for ^{12}C and 7.0 for $^{\rm nat}$Pb.

Protons interact at about $\frac{1}{3}$ nuclear matter density for all our targets except lithium. This density determines the average Fermi momentum of the struck nucleon, which in turn determines the width of the quasielastic peak. We therefore expect the ^{12}C and $^{\rm nat}$Pb quasielastic peaks to exhibit roughly the same width.

A recent publication by Depace and Viviani [24] has examined the 795-MeV quasielastic data using a surface type response. They have also calculated a two-step con-

tribution. While the shape of their two-step curve is similar to ours, it is smaller by nearly a factor of 2. This discrepancy may result from the different values of $\sigma_{\rm tot}$ used in the two calculations. The two-step distortion factor is very sensitive to this quantity. In our calculations at 795 MeV the in-medium value of 32 mb was used instead of the full 40 mb. In addition, values of the NN cross sections used in these two calculations may differ. Our calculations were done in a similar framework to those in Ref. [38] and are consistent with the calculations illustrated in that reference.

V. COMPARISON OF DATA TO THE MODELS

A. Cross section

Plotted in Figs. 4–7, are the results of the one-step slab model calculations added to the two-step contribution. The calculations for 495 MeV are all multiplied by 1.3, while the calculations for 795-MeV ^{12}C and $^{\rm nat}$Pb required a normalization factor of 1.8. In addition, all the calculations are shifted to higher energy loss to align them with the quasielastic peak position. The calculations are able to account very well for the shape of the quasielastic peak at both energies for both ^{12}C and $^{\rm nat}$Pb. This is a distinguishing feature of the slab model. Compared to Fermi-gas calculations the slab calculation puts a long tail on the high-energy-loss side of the quasielastic peak and fills in the region of low energy loss where Fermi-gas calculations produce a sharp cutoff.

The two-step contribution does not significantly alter the shape of the calculation, but it does add substantial cross section at the largest momentum transfers. For example, two-step scattering contributes nearly a third of the cross section at 24° (3.0 fm^{-1}) and 28° (3.5 fm^{-1}) at 795 MeV. Without the two-step contribution, a single angle-independent normalization factor will not bring the calculations into close agreement with the magnitude of the quasielastic cross section.

The single-step slab model cross section plus two-step Fermi-gas contribution for the ^{12}C(p,n) reaction is shown in the top panels of Fig. 12 for 495 MeV and Fig. 13 for 795 MeV. The same is shown for the $^{\rm nat}$Pb(p,n) reaction at 795 MeV in Fig. 14. In these figures the individual single-step and two-step distributions are shown.

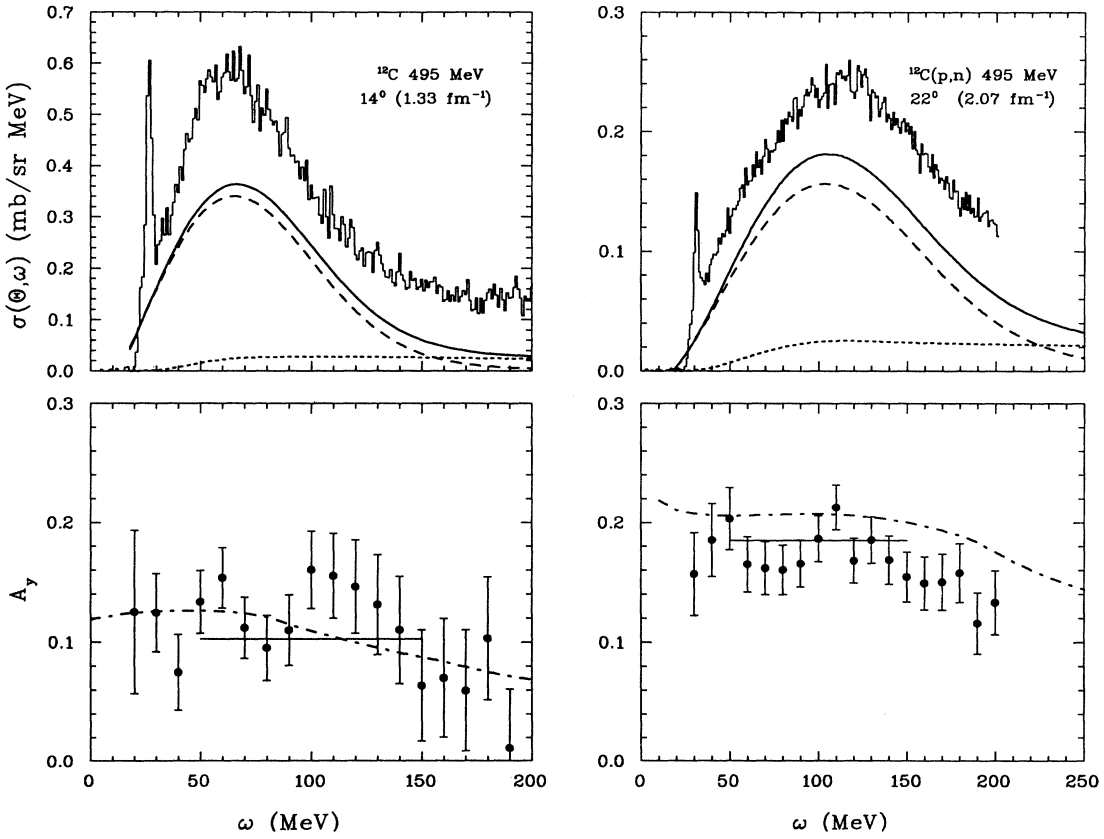

FIG. 12. The top panels show the energy loss cross section spectrum for ^{12}C at 14° (left) and 22° (right) at 495 MeV. The dashed line is the slab model contribution and the dotted line is the two-step contribution. The solid line is the sum of these. The model curves have all been shifted by 18 MeV to higher excitation. Below the cross section spectra are the analyzing-power measurements for the same energy and angle. The horizontal solid line is the analyzing power for the free (p,n) reaction taken from Ref. [23]. The dash-dotted line is the RPWIA calculation from Ref. [37].

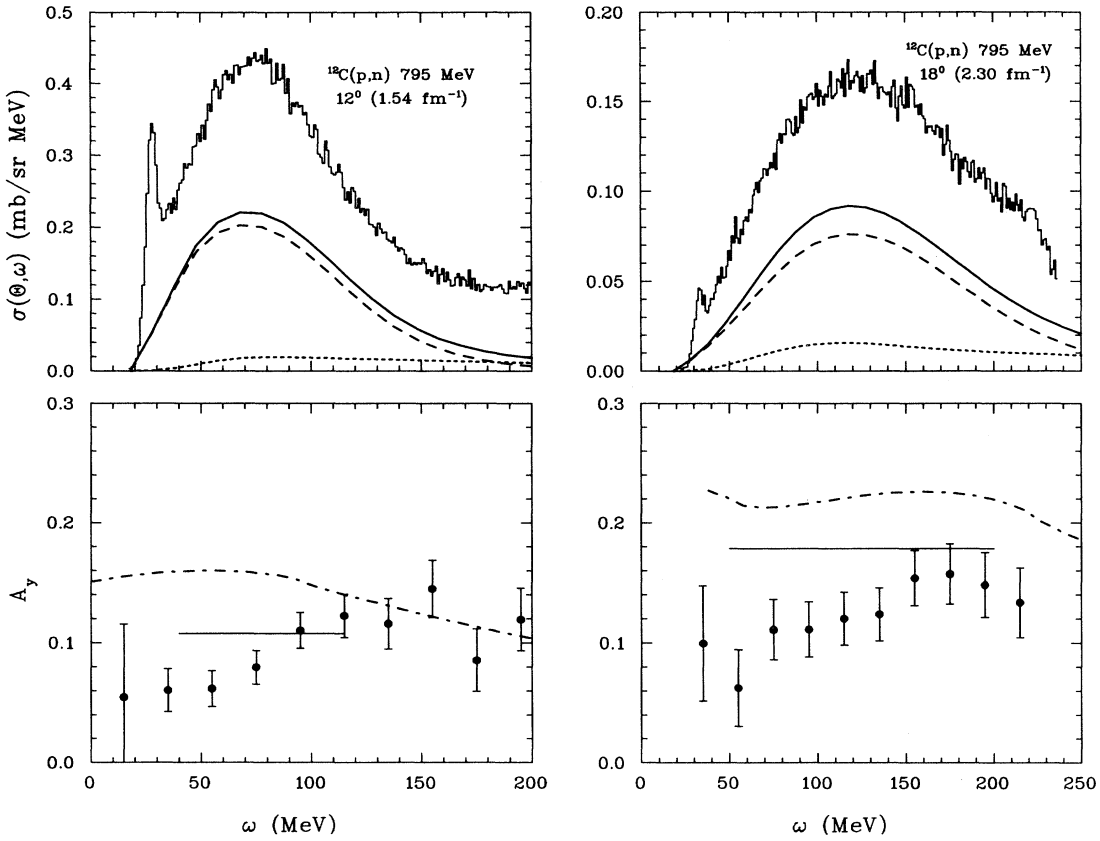

FIG. 13. The same as Fig. 12 except that it is for the ^{12}C$(\vec{p},n)$ reaction at 12° (left) and 18° (right) at 795 MeV.

The calculations are shifted in all figures to match the quasielastic peak position, but the magnitude of the calculated cross sections has not been renormalized.

The shift in the model curves was accomplished by simply sliding the curve until the curve was aligned with the data around the region of the quasielastic peak. Because the slab model incorporates collective effects in the RPA, the peak position of the unshifted model curves has a different momentum transfer dependence than that for free NN kinematics. Therefore, the amount the model curve was shifted depended on the momentum transfer. At low **q** the shift was approximately 10 MeV, whereas at the largest **q** the model curves had to be shifted by as much as 30 MeV.

The calculated contribution from two-step scattering relative to one-step scattering at 495 MeV is similar to the relative contribution at 795 MeV, despite the fact that the actual number of effective pairs (N_{double}) for two-step scattering at 495 MeV is larger by 30% than at 795 MeV. For two-step scattering each charge exchange is preceded or followed by an elastic NN scattering. One reason the calculated two-step contribution is reduced at 495 MeV is that elastic NN scattering is smaller by almost a factor of 2 at 495 MeV than its value at 795 MeV, while the charge-exchange NN cross section changes very little. These figures also show that the calculated two-step contribution becomes a larger fraction of the cross section as the angle increases, as was expected.

To directly compare the $^{\text{nat}}$Pb and ^{12}C data, we have divided the cross section by the effective number of neutrons N_{eff} for each target. If the reaction is predominantly one step and the Glauber description of distortion effects is a reasonable approximation, the spectra should coincide in the quasielastic region. The $^{\text{nat}}$Pb and ^{12}C spectra divided by N_{eff} are overlaid in Fig. 15 and good agreement is obtained at 12° (1.5 fm^{-1}). At 20° (2.6 fm^{-1}) the $^{\text{nat}}$Pb data are somewhat larger than the ^{12}C data. This could be because of two-step scattering. The calculated two-step contribution is larger in $^{\text{nat}}$Pb than in ^{12}C and at the larger angle the two-step contribution will make up a larger part of the cross section. Thus the spectra will no longer scale with N_{eff}. At 495 MeV the target dependence of two-step scattering should be much greater, so it would be interesting to make the same sort of comparison of ^{12}C and $^{\text{nat}}$Pb at large angles at this energy.

B. Analyzing power

Figure 12 shows our analyzing power measurements for ^{12}C at 495 MeV and 14° (1.3 fm^{-1}) and 22° (2.1 fm^{-1}). The dashed line is the free NN analyzing power

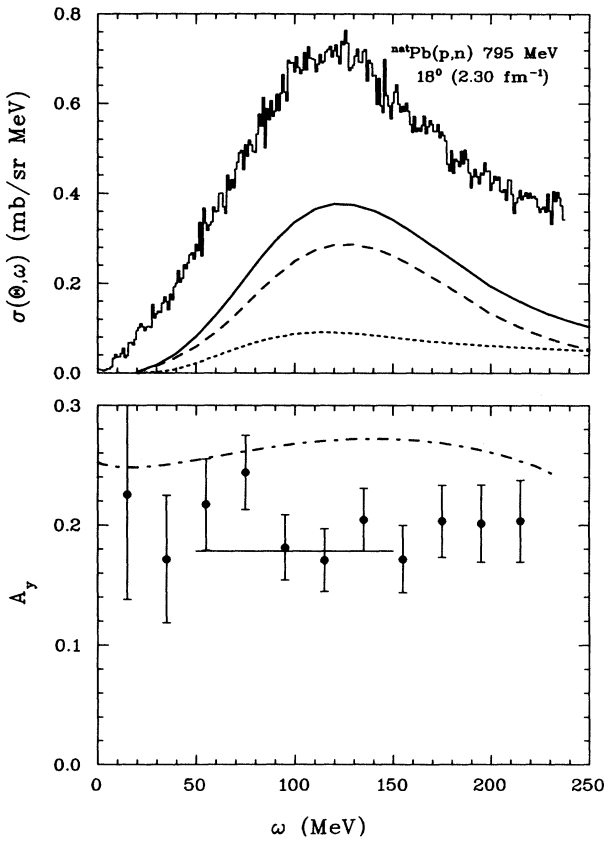

FIG. 14. The same as Fig. 12 except that it is for the ^{nat}Pb$(\vec{p},n)$ reaction at 18° and 795 MeV.

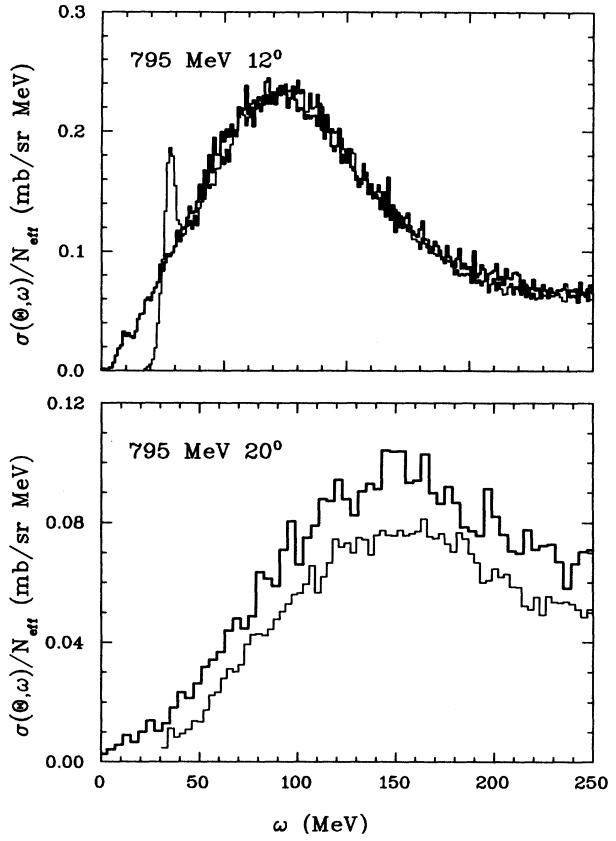

FIG. 15. ^{12}C (light) and ^{nat}Pb (dark) cross section spectra divided by $N_{\rm eff}$ as determined for each nucleus by expression (4.2). The top panel shows the 12° data and the bottom is the 20° data.

obtained from the FA92 phase-shift solution of Arndt and Roper [23]. In both panels the quasielastic analyzing power is consistent with the free charge-exchange value. The relativistic calculation with pseudovector coupling is in agreement with the data at 14°, but is slightly high at 22°.

The analyzing power for ^{12}C at 795 MeV is shown in Fig. 13. At this energy, the data are below the free NN value at the low-energy-loss side of the peak and then rise up to about the free value at higher energy loss. On average, however, the quasielastic analyzing power is significantly below the free value and well below a relativistic calculation.

Figure 14 shows the ^{nat}Pb analyzing power at 18° (2.3 fm^{-1}) at 795 MeV. In contrast to the ^{12}C data, the ^{nat}Pb data are consistent with the free NN value. A similar trend was also reported by Hicks *et al.* [27]. The analyzing power is larger in ^{54}Fe(p,n) than in ^{12}C(p,n) at 420 MeV on the low-energy-loss side of the quasielastic peak. This was attributed to nuclear structure effects.

The average analyzing power over the quasielastic peak region is plotted in Fig. 16 for ^{12}C at 495 MeV and for ^{12}C and ^{nat}Pb at 795 MeV. This figure demonstrates that the same tendencies apply for all the angles studied. Both the 495-MeV ^{12}C and 795-MeV ^{nat}Pb data are consistent with free scattering while the 795-MeV ^{12}C data are below the free value.

VI. DISCUSSION

The data presented here demonstrate that there is relatively little energy or target dependence to the general features of the quasielastic double differential cross section. This is consistent with the Glauber approximation which predicts about the same average density of interaction for ^{12}C and ^{nat}Pb at 795 MeV and ^{12}C at 495 MeV. Properties such as the width of the quasielastic peak should therefore be similar.

While several general aspects of the quasielastic peak are described by the simple models used here, one problem that remains unresolved is an explanation for the magnitude of the differential cross section. Even with a contribution from two-step scattering the slab model was unable to account for much more than two thirds of the cross section. This is true even at 495 MeV where the agreement between our ^{2}H data and the free NN cross section is good.

We have compared our cross section data to the slab

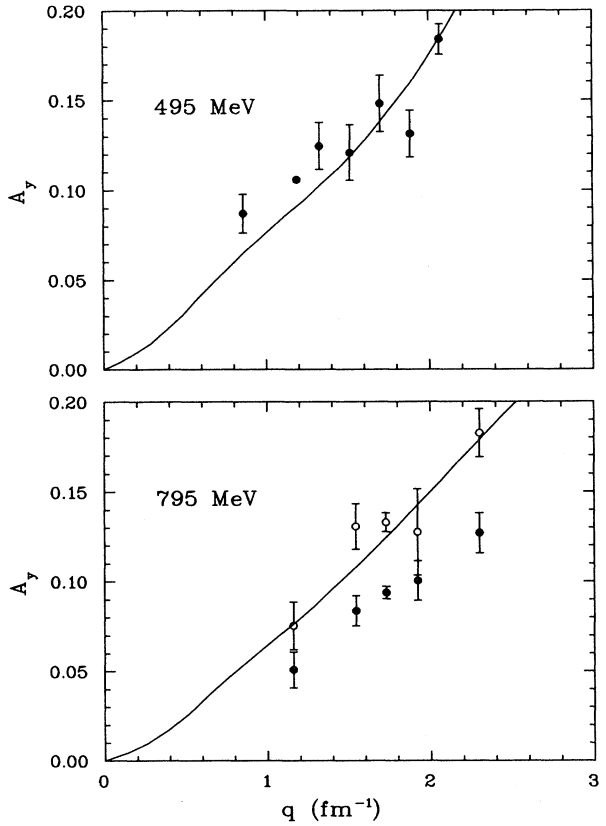

FIG. 16. The top panel shows the average analyzing power over the quasielastic peak region for ^{12}C at 495-MeV (solid circles). The bottom panel shows this quantity for ^{12}C and ^{nat}Pb (open circles) at 795 MeV. The solid lines show the analyzing power from SAID [23]. The 495-MeV carbon point at 1.2 fm^{-1} and the Pb data at 1.73 fm^{-1} and 795 MeV were taken during updates to LAMPF experiment 881 [8].

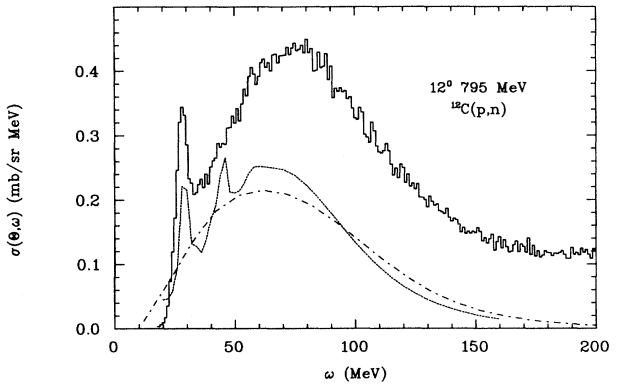

FIG. 17. A comparison of the slab model and the finite-nucleus distorted-waves calculation of Ref. [42]. The calculations are for carbon at 12° and 795 MeV. The dotted curve is the finite-nucleus calculation and the dot-dashed curve is from the slab model. Our data are shown along with the curves. Both calculations were shifted 10 MeV to higher energy loss to align the 4^- state in the finite-nucleus calculation with the data.

model because this code is available and easy to run. However, there exist recent very detailed calculations of the quasielastic cross section [41,42]. These distorted-waves finite-nucleus calculations include correlations in the RPA. We compare in Fig. 17 the slab model calculation with a finite-nucleus calculation for carbon from Ref. [43] in order to assess the effects of using the simpler slab model to describe our data. These calculations are shown at 795 MeV and 12° along with our data for this energy and angle. Both model curves were shifted 10 MeV in order to align the 4^- state in the finite-nucleus model with this state in the carbon data.

The two curves differ in the region of low ω where discrete states and giant resonances are found. Also, the slab model produces a slightly wider distribution. However, the magnitude of the cross section and the position of the quasielastic peak are very similar in the two models.

The calculated curves are driven by the free NN amplitudes. The integrated cross sections for our ^{2}H data at 795 MeV are a factor of 1.2 times larger than the cross sections derived from the phase shifts. However, even if we multiply the model curves by this number, they still are well below the data.

The discrepancy between cross sections calculated with nonrelativistic distorted-waves codes and (p,n) charge-exchange data has been noted before [42] and attributed to multiple scattering processes. We note that even the more elaborate calculation of two-step scattering done in Ref. [24] cannot account for the extra cross section in this region. Models of the two-step contribution more sophisticated than that presented here or in Ref. [24] are needed. In addition, meson-exchange currents have been shown to be important for describing (e,e') quasielastic scattering [44]. These types of processes may also make a contribution to (p,n) quasielastic scattering and could account for some of the missing strength in this region.

The 495-MeV analyzing-power data essentially agree with the free NN scattering at all angles, consistent with the results of Ref. [8]. However, the analyzing power for ^{12}C(p,n) at 795 MeV is below the free values and varies with energy loss in a way not predicted by any theory. In fact, the RPWIA predicts the analyzing power should be enhanced rather than suppressed.

The analyzing power data for ^{nat}Pb at 795 MeV agrees with the free NN values in contrast to the 795-MeV ^{12}C data. This target dependence possibly indicates that there are nuclide-dependent distortion effects or that nuclear structure effects are still important even at these large momentum transfers.

Measurements of quasielastic scattering using the (p,p') reaction at 500 MeV show a large (40%) suppression in the analyzing power from the free NN value [9]. The RPWIA is able to describe these data fairly well. It may be that reactions that are sensitive to the isoscalar part of nuclear response are more sensitive to relativistic effects than is the (p,n) reaction.

The most significant result of this set of data is the momentum transfer dependence of the quasielastic peak position. The peak position is shifted to larger energy loss relative to free NN scattering by 18–25 MeV on all targets over the full range of momentum transfer studied here. This is in contrast to the $(^3\mathrm{He}, t)$ reaction, which shows a dramatic shift toward lower energy loss at about 2 fm^{-1}. The (p, n) data cast doubts on the suggestion that longitudinal correlations are the cause of this momentum transfer dependence in the $(^3\mathrm{He}, t)$ data [4]. Recently, Dimetriev [45] has shown that distortions involved with this complex probe may be responsible for the behavior of the $(^3\mathrm{He}, t)$ data.

The data presented here lead to a generalization of the conclusion reached in the polarization-transfer study [8]. In that work, a separation of the transverse and longitudinal responses was accomplished at 495 MeV and 1.72 fm^{-1}. It was shown that both the transverse and longitudinal responses are shifted to higher energy loss from the free NN kinematics by 30 MeV and 20 MeV, respectively. The present data suggest that little or no change in the peak positions of the separated responses will be found at either larger or smaller momentum transfers. Furthermore, these data indicate that no significant changes should be observed in the peak positions of the responses at higher energies.

While many of the features of these quasielastic data may be accounted for with models using the nuclear matter approximation, the interesting deviations of our data from these models show that more extensive theoretical calculations for finite nuclei including multiple scattering are necessary.

The difference in peak position for the (p, p') and (p, n) reactions has been explained through sum rules in Refs. [33,34]. The exact calculations in Ref. [33] upon which the sum rules calculations are based have been able to describe both the longitudinal and transverse parts of quasielastic (e, e') scattering on ^{4}He [46,47]. These calculations do not contain the approximations that are assumed in more traditional models and include $2p$-$2h$ and higher-order processes. Such calculations for the (p, n) reaction on heavier nuclei are needed.

ACKNOWLEDGMENTS

We wish to thank Dr. J. Piekarewicz for allowing us to use his RPWIA code and Dr. Thomas Sams for providing us with the finite-nucleus calculations. This work was supported in part by the National Science Foundation and the U.S. Department of Energy.

[1] F. Osterfeld, Rev. Mod. Phys. **64**, 491 (1992).
[2] W.M. Alberico, M. Ericson, and A. Molinari, Nucl. Phys. **A379**, 429 (1982).
[3] J.S. O'Connell and B. Schrøder, Phys. Rev. C **38**, 2447 (1988).
[4] J. Bergqvist *et al.*, Nucl. Phys. **A469**, 648 (1987).
[5] R.E. Chrien *et al.*, Phys. Rev. C **21**, 1014 (1980).
[6] T.A. Carey, K.W. Jones, J.B. McClelland, J.M. Moss, L.B. Rees, N. Tanaka, and A.D. Bacher, Phys. Rev. Lett. **53**, 144 (1984).
[7] L.B. Rees, J.M. Moss, T.A. Carey, K.W. Jones, J.B. McClelland, N. Tanaka, A.D. Bacher, and H. Esbensen, Phys. Rev. C **34**, 627 (1986).
[8] X.Y. Chen, T.N. Taddeucci, W.P. Alford, M. Barlett, R.C. Byrd, T.A. Carey, D.E. Ciskowski, C.C. Foster, C. Gaarde, C.D. Goodman, C.A. Goulding, E. Gülmez, W. Huang, D.J. Horen, J. Larsen, D. Marchlenski, J.B. McClelland, D. Prout, J. Rapaport, L.J. Rybarcyk, W.C. Sailor, E. Sugarbaker, and C.A. Whitten, Jr., Phys. Rev. C **41**, 2548 (1990).
[9] C.J. Horowitz and D.P. Murdock, Phys. Rev. C **37**, 2032 (1988).
[10] J.B. McClelland, D.A. Clark, J.L. Davis, R.C. Haight, R.W. Johnson, N.S.P. King, G.L. Morgan, L.J. Rybarcyk, J. Ullmann, P. Lisowski, W.R. Smythe, D.A. Lind, C.D. Zafiratos, and J. Rapaport, Nucl. Instrum. Methods Phys. Res. Sect. A **276**, 35 (1989).
[11] E.P. Chamberlin, R.L. York, H.E. Williams, and E.L. Rios, in *Polarization Phenomena in Nuclear Physics-1980*, edited by G.G. Ohlsen, Ronald E. Brown, Nelson Jarmie, M.W. McNaughton, and G.M. Hale, AIP Conf. Proc. No. 69 (American Institute of Physics, New York, 1981), p. 887.
[12] J.B. McClelland, Can. J. Phys. **65**, 633 (1987); in *Spin Observables of Nuclear Probes*, Proceedings of the International Conference on Spin Observables of Nuclear Probes, Telluride, CO, 1988, edited by C.J. Horowitz, C.D. Goodman, and G. Walker (Plenum, New York, 1989), p. 183.
[13] D.A. Lind, Can. J. Phys. **65**, 637 (1986).
[14] R.L. York, O.B. van Dyck, D.R. Swenson, and D. Tupa, in Proceedings of the International Workshop on Polarized Ion Sources and Polarized Gas Jets, Tsukuba, Japan, 1990 (KEK 90-15), p. 170.
[15] T.N. Taddeucci, W.P. Alford, M. Barlett, R.C. Byrd, T.A. Carey, D.E. Ciskowski, C.C. Foster, C. Gaarde, C.D. Goodman, C.A. Goulding, E. Gülmez, W. Huang, D.J. Horen, J. Larsen, D. Marchlenski, J.B. McClelland, D. Prout, J. Rapaport, L.J. Rybarcyk, W.C. Sailor, E. Sugarbaker, and C.A. Whitten, Jr., Phys. Rev. C **41**, 2548 (1990).
[16] L.J. Rybarcyk, "Progress at LAMPF January–December 1988," Report No. LA–11670-PR, 1989, p. 48.
[17] B.E. Bonner, J.E. Simmons, C.R. Newsom, P.J. Riley, G. Glass, J.C. Hiebert, M. Jain, and L.C. Northcliffe, Phys. Rev. C **18**, 1418 (1978).
[18] C.W. Bjork *et al.*, Phys. Lett. **63B**, 31 (1976).
[19] C.G. Cassapakis *et al.*, Phys. Lett. **63B**, 35 (1976).
[20] R.G. Jeppesen, Ph.D. thesis, University of Colorado, 1986.
[21] D.L. Prout, Ph.D. thesis, University of Colorado, 1992.
[22] B.E. Bonner, J.E. Simmons, J.M. Wallace, M.L. Evans,

G. Glass, J.C. Hiebert, M. Jain, L.C. Northcliffe, C.W. Bjork, P.J. Riley, and C.G. Cassapakis, Phys. Rev. C **17**, 664 (1978).
[23] R.A. Arndt and L.D. Roper, "Scattering Analyses Interactive Dial-in program (SAID)," Virginia Polytechnic Institute and State University report, 1992 (unpublished); phase-shift solution FA92.
[24] A. De Pace and M. Viviani, Phys. Rev. C **48**, 2931 (1993).
[25] A. Erell *et al.*, Phys. Rev. C **34**, 1822 (1986).
[26] R.J. Peterson, S. Høbråten, J. Ouyang, M.R. Braunstein, X.Y. Chen, M.D. Kohler, B.J. Kriss, D.J. Mercer, D.S. Oakley, and D.L. Prout, Phys. Lett. B **297**, 238 (1992).
[27] K.H. Hicks, W.P. Alford, A. Celler, R.S. Henderson, K.P. Jackson, C.A. Miller, M.C. Vetterli, S. Yen, F. Brieva, C.J. Horowitz, and J. Piekarewicz, Phys. Rev. C **47**, 260 (1993).
[28] J.A. McGill, G.W. Hoffmann, M.L. Bartlett, R.W. Fergerson, E.C. Milner, R.E. Chrien, R.J. Sutter, T. Kozlowski, and R.L. Stearns, Phys. Rev. C **29**, 204 (1984).
[29] E.J. Moniz, I. Sick, T.T. Whitney, J.R. Ficenec, R.D. Kephart, and W.P. Trower, Phys. Rev. Lett. **26**, 445 (1971).
[30] T.W. Donnelly and J.D. Walecka, Annu. Rev. Nucl. Sci. **25**, 329 (1975).
[31] R. Rosenfelder, Phys. Lett. **79B**, 15 (1978).
[32] A. De Pace and M. Viviani, Phys. Lett. B **254**, 20 (1991).
[33] V.R. Pandharipande, J. Carlson, Steven C. Pieper, R.B. Wiringa, and R. Schiavilla, Phys. Rev. C **49**, 789 (1994).
[34] J. Wambach, Phys. Rev. C **46**, 807 (1992).
[35] A.L. Fetter and J.D. Walecka, *Quantum Theory of Many Particle Systems* (McGraw-Hill, New York, 1971).
[36] R.D. Smith, in *Spin Observables of Nuclear Probes* [12], p. 15.
[37] C.J. Horowitz and J. Piekarewicz, Phys. Lett. B **301**, 321 (1993).
[38] H. Esbensen and G.F. Bertsch, Phys. Rev. C **32**, 553 (1985).
[39] C.W. de Jager, H. de Vries, and C. de Vries, At. Data Nucl. Data Tables **14**, 479 (1974).
[40] R.D. Smith and M. Bozoian, Phys. Rev. C **39**, 1751 (1989).
[41] M. Ichimura, K. Kawahigashi, T.S. Jørgensen, and C. Gaarde, Phys. Rev. C **39**, 1446 (1989).
[42] T. Sams, in *Proceedings of the RIKEN International Workshop on Delta Excitations in Nuclei*, Tokyo, Japan, 1993, edited by M. Ichimura, H. Toki, and M. Ishihara (World Scientific, Singapore, 1994), p. 301. (The nuclear response function used in these calculations was provided by the authors of Ref. [41].)
[43] T. Sams (private communication). The nuclear response function used in these calculations was from [41].
[44] W.M. Alberico, M. Ericson, and A. Molinari, Ann. Phys. (N.Y.) **154**, 356 (1984).
[45] V.F. Dimetriev, Phys. Lett. B **226**, 219 (1989).
[46] J. Carlson and R. Schiavilla, Phys. Rev. Lett. **68**, 3682 (1992).
[47] J. Carlson and R. Schiavilla, Phys. Rev. C **49**, 2880 (1994).